의학박사 학위논문

AICAR upregulates ABCA1/ABCG1 expression in the retinal pigment epithelium and reduces Bruch's membrane lipid deposit in ApoE deficient mice

ApoE 유전자 결손 생쥐에서 AICAR 약물에 의한
망막색소상피세포의 ABCA1/ABCG1 발현 증가 및
브루크막의 지질 침착 감소 효과 분석

2022년 8월

서울대학교 대학원

의학과 안과학 전공

김 용 규

AICAR upregulates ABCA1/ABCG1 expression in the retinal pigment epithelium and reduces Bruch's membrane lipid deposit in ApoE deficient mice

지도 교수 박 규 형

이 논문을 의학박사 학위논문으로 제출함
2022년 4월

서울대학교 대학원
의학과 안과학 전공
김 용 규

김용규의 의학박사 학위논문을 인준함
2022년 7월

위 원 장	김 태 우	(인)
부위원장	박 규 형	(인)
위 원	현 준 영	(인)
위 원	연 태 진	(인)
위 원	최 경 식	(인)

ABSTRACT

The etiology of age-related macular degeneration (AMD) is diverse; however, recent evidence suggests that the lipid metabolism-cholesterol pathway might be associated with the pathophysiology of AMD. The ATP-binding cassette (ABC) transporters, ABCA1 and ABCG1, are essential for the formation of high-density lipoprotein (HDL) and the regulation of macrophage cholesterol efflux. The failure of retinal or retinal pigment epithelium (RPE) cholesterol efflux to remove excess intracellular lipids causes morphological and functional damage to the retina. In this study, we investigated whether treatment with 5-aminoimidazole-4-carboxamide ribonucleotide (AICAR), an AMP-activated protein kinase (AMPK) activator, improves RPE cholesterol efflux and Bruch's membrane (BM) lipid deposits. The protein and mRNA levels of ABCA1 and ABCG1 in ARPE-19 cells and retinal and RPE/choroid tissue from apolipoprotein E-deficient ($ApoE^{-/-}$) mice were evaluated after 24 weeks of AICAR treatment. The cholesterol efflux capacity of ARPE-19 cells and the cholesterol-accepting capacity of apoB-depleted serum from mice were measured. The thickness of the BM and the degree of lipid deposition were evaluated using electron microscopy. AICAR treatment increased the phosphorylation of AMPK and the protein and mRNA expression of ABCA1 and ABCG1 in vitro. It promoted cholesterol efflux from ARPE-19 cells and upregulated the protein and mRNA levels of ABCA1 and ABCG1 in the retina and RPE in vivo. ApoB-depleted serum from the AICAR-treated group showed enhanced cholesterol-accepting capacity. Long-term treatment with AICAR reduced BM thickening and lipid deposition in $ApoE^{-/-}$ mice. In conclusion, AICAR treatment increased the expression of lipid transporters in the retina and RPE in

vivo, facilitated intracellular cholesterol efflux from the RPE in vitro, and improved the functionality of HDL to accept cholesterol effluxed from the cell, possibly via AMPK activation. Collectively, these effects might contribute to the improvement of early age-related pathologic changes in the BM. Pharmacological improvement of RPE cholesterol efflux via AMPK activation may be a potential treatment strategy for AMD.

Keywords: AICA ribonucleotide; AMP-Activated Protein Kinases; ATP-Binding Cassette Transporters; Cholesterol; Macular Degeneration; Retinal Pigment Epithelium

Student Number: 2014-30636

CONTENTS

LIST OF TABLES AND FIGURES

LIST OF ABBREVIATIONS

ABC, ATP-binding cassette

ACC, Acetyl-CoA carboxylase

AICAR, 5-aminoimidazole-4-carboxamide ribonucleotide

AMD, Age-related macular degeneration

AMPK. AMP-activated protein kinase

ApoB, Apolipoprotein B

ApoE, Apolipoprotein E

$ApoE^{-/-}$, apolipoprotein E-deficient

ATCC, American Type Culture Collection

BM, Bruch's membrane

cDNA, complementary deoxyribonucleic acid

DMEM, Dulbecco's Modified Eagle's Medium

EL, Electron-lucent

HDL, High-density lipoprotein

LDL, Low-density lipoprotein

LXR, Liver X receptor

PEG, Polyethylene glycol

qRT-PCR, Quantitative real-time polymerase chain reaction

RPE, Retinal pigment epithelium

RNA, Ribonucleic acid

WST-1, Water-soluble tetrazolium salt-1

INTRODUCTION

Age-related macular degeneration (AMD) is a vision-threatening disorder in the elderly population worldwide.[1] The etiology of AMD is diverse; however, recent genome-wide association studies have shown that genomic polymorphisms associated with lipid metabolism are a risk factor for AMD. Thus, the lipid metabolism-cholesterol pathway may be associated with the pathophysiology of AMD.[2-10] Drusen is an extracellular deposit located between the basal lamina of the retinal pigment epithelium (RPE) and inner collagenous layer of Bruch's membrane (BM). The biological process of BM lipid deposition shares several aspects with atherosclerosis.[11, 12] Reverse cholesterol transport is the active removal of surplus cholesterol from the cell, mediated by high-density lipoprotein (HDL), which prevents the progression of atherosclerosis.[13] The ATP-binding cassette (ABC) transporters ABCA1 and ABCG1 are essential for the formation of HDL and modulation of macrophage cholesterol efflux.[14]

ABCA1 and ABCG1 are found in the retina, RPE, and macrophages.[15, 16] The cholesterol efflux capacities of these cells are crucial for maintaining lipid homeostasis in the retina and are known to exhibit retinal degeneration in cases of deterioration. The specific suppression of both ABCA1 and ABCG1 in rod photoreceptors or RPE resulted in lipid aggregation in the RPE and degeneration of RPE and photoreceptors.[17, 18] In addition to retinal and RPE cells, the targeted deletion of ABCA1 and ABCG1 in macrophages also results in extracellular lipid accumulation in the subretinal space.[19] This suggests that the failure of cholesterol efflux to remove excess intracellular lipids from the retina, a lipid-rich environment, causes morphological and functional damage to the retina. Thus, it is

necessary to establish an approach to improve cholesterol efflux in these cells and determine whether this could improve the pathology of AMD.

AMP-activated protein kinase (AMPK) controls cellular energy balance and is activated when cellular energy levels are low.[20] AMPK inhibits foam cell formation during the early stages of atherosclerosis.[21] AMPK activation enhances the cholesterol efflux capacity of macrophages by upregulating ABCA1 and liver X receptor (LXR)-α, an upstream transcriptional activator.[22] A nucleoside similar to adenosine, 5-aminoimidazole-4-carboxamide ribonucleotide (AICAR), and its metabolite 5-aminoimidazole-4-carboxamide ribotide, are 5'-AMP analogs that emulate various cellular effects of AMP. AICAR has been widely used to investigate the cellular function of AMPK.[23] Treatment with AICAR induces increased AMPK phosphorylation and ABCA1 formation and promotes macrophage cholesterol efflux.[24] AMPK activation increases cholesterol uptake and excretion in the liver, as well as cholesterol transport from peripheral macrophages to the systemic circulation, thereby reducing the formation of atherosclerotic plaques in the apolipoprotein E-deficient ($ApoE^{-/-}$) mouse aorta.[25]

Different types of apolipoprotein E (ApoE) alleles are associated with AMD.[26, 27] $ApoE^{-/-}$ mice exhibited high levels of plasma cholesterol, and histological examination revealed that these mice developed BM thickening, which was accompanied by the accumulation of electron-lucent (EL) particles and membrane-bound vacuoles, which have an ultrastructural appearance similar to that of membranous debris found in basal linear deposits at an earlier age.[28, 29] Here, we investigated whether AICAR treatment could affect the expression of lipid transporters and improve RPE cholesterol efflux via AMPK activation in ARPE-19

cells. We also used $ApoE^{-/-}$ mice as a model for dry AMD to determine whether AICAR treatment could improve BM lipid deposition.

MATERIALS AND METHODS

1) Cell culture

ARPE-19 cells were purchased from American Type Culture Collection (ATCC, CRL-2302) and maintained in Dulbecco's Modified Eagle's Medium (DMEM) /F12 (Gibco, CA, USA) supplemented with 10% fetal bovine serum (Gibco) and 1% penicillin/streptomycin (Gibco). The cells were grown in a 37 °C humidified 5% CO_2 incubator.

2) Water-soluble tetrazolium salt-1 (WST-1) cell viability assay

The influence of AICAR, an AMP mimetic activator of AMPK, and Compound C, an AMPK inhibitor, on cell viability was assessed using a WST-1 assay kit (EZ-Cytox, DoGen, Seoul, Korea). In brief, 5×10^3 ARPE-19 cells per well were cultured in a 96-well plate, and cells were pretreated with various concentrations of Compound C (#S7306, Selleckchem, Houston, TX, USA) for 30 min and then with 0.5 mM or 1 mM AICAR (#S1802, Selleckchem). After 24 h, the cell viability was assessed by measuring the absorbance at 450 nm. All experiments were performed in triplicate.

3) Animals

ApoE-deficient ($ApoE^{-/-}$) male mice on a C57BL/6 background (age, 8 weeks old; weight, 23-25 g) and C57BL/6J male mice (age, eight-weeks-old; weight, 23-25 g) were purchased from the Jackson Laboratory (Bar Harbor, ME, USA). The animals were treated according to the ARVO Statement for the Use of Animals in Ophthalmic and Vision Research. The study was approved by the Institutional

Animal Care and Use Committee of Seoul National University Bundang Hospital. $ApoE^{-/-}$ mice were fed a high-fat diet (60% kcal fat, D12492, Research Diets, Inc., NJ, USA) and C57BL/6J mice were fed a normal diet (rodent chow). Mice were kept in a specific-pathogen-free laboratory animal facility under a 12 h light/12 h dark cycle. Mice were treated with either AICAR (200 mg/kg, i.p., Item No.10010241, Cayman Chemical, MI, USA) or normal saline (100 μL, i.p.) once per day for 24 weeks. Mice were classified into three groups: Group A ($ApoE^{-/-}$ mice injected with normal saline, n = 12), Group B ($ApoE^{-/-}$ mice injected with AICAR, n = 12), and Group C (C57BL/6J mice injected with normal saline, n = 12). Three mice in each group were sacrificed at 14 weeks for interim optical coherence tomography angiography and electron microscopy analysis. The remaining mice were sacrificed 24 weeks after the initial treatment.

4) Western blot analysis

ARPE-19 cell lysate and retinal and RPE/choroidal tissue from mice were used for western blot analysis. ARPE-19 cells (passage number 3 or 4) were grown in a 100 mm cell culture dish. When more than 90% confluency was reached, cells were pretreated with or without 5 μM Compound C (#S7306, Selleckchem) for 30 min. Cells were treated with or without 0.5 mM of AICAR (#S1802, Selleckchem) diluted in dimethyl sulfoxide. After 16 h, cells were harvested and proteins were extracted using protein extraction solution (PRO-PREP, #17081, Intron Biotechnology, Seongnam, Korea). The mouse eyeball was enucleated after CO_2 euthanasia. The corneal cup was dissected, and the retinal and RPE/choroidal tissues were carefully extracted. The tissue was ground using a conical tissue

grinder. Bradford assay was used for protein quantification. Equal amount of protein (15 μg) was loaded onto sodium dodecyl sulfate-polyacrylamide gels. Primary antibodies targeting ABCA1 (sc-58219, Santa Cruz, CA, USA), ABCG1 (ab52617, Abcam, MA, USA), SR-BI (ab217318, Abcam), LXR-α (ab41902, Abcam), acetyl-CoA carboxylase (ACC) (#3676, Cell Signaling Technology, MA, USA), phospho-ACC (Ser79, #3661, Cell Signaling Technology), AMPK (#2532, Cell Signaling Technology), phospho-AMPK (#2531, Cell Signaling Technology), and β-actin (sc-47778, Santa Cruz, CA, USA) were diluted (1:1,000) in blocking buffer (Tris-buffered saline with Tween-20; Biosesang, Gyeonggi, Korea) with 5% nonfat milk (Difco; Becton-Dickinson and Co., Sparks, MD, USA). Goat anti-mouse (#1706516, Bio-Rad, CA, USA) or anti-rabbit IgG (#1706515; Bio-Rad) were used as secondary antibodies. Signals were visualized using the chemiluminescent image analysis system (Bio-Rad), and densitometry was quantified using Image J (National Institutes of Health, Bethesda, MD, USA).

5) Quantitative real-time polymerase chain reaction (qRT-PCR)

qRT-PCR was performed using the ARPE-19 cell lysate, retinal and RPE/choroidal tissue from mice, and SYBR Green (WizPure Bio, Seoul, Korea). Total RNA was extracted using TRIzol reagent (Invitrogen, Carlsbad, CA, USA) and reverse transcribed into cDNA using reverse transcriptase. The sequences of the primers used for qRT-PCR are listed in Table 1. Expression levels were normalized to that of GAPDH.

Table 1. Oligonucleotide primer sequences for quantitative PCR

Gene	Direction	Sequence	Annealing temperature (℃)	Product size (bp)
ABCA1	Forward	5'-GTGTGGGCTCCTCCCTGTTT-3'	60	205
	Reverse	5'-TCGATGGTCAGCGTGTCACT-3'		
ABCG1	Forward	5'-AGGTCTCCAATCTCGTGCCG-3'	60	119
	Reverse	5'-GCGACTGTTCTGATCCCCGT-3'		
LXR-α	Forward	5'-AGGAGTGTCGACTTCGCAAA-3'	60	158
	Reverse	5'-CTCTTCTTGCCGCTTCAGTTT-3'		
GAPDH	Forward	5'-GGTCTCCTCTGACTTCAACA-3'	60	116
	Reverse	5'-AGCCAAATTCGTTGTCATAC-3'		

6) Serum analyses

Blood samples were collected from the cardiac ventricles of the mice after 24 weeks of treatment. The levels of serum total cholesterol, triglycerides, low-density lipoprotein (LDL), and HDL were measured using a semi-automated enzymatic method with a Beckman Coulter AU analyzer (AU 680; Beckman Coulter, Brea, CA, USA).

7) Cholesterol efflux capacity

We measured the ability of ARPE-19 cells to export cholesterol and the functionality of mice serum deprived of apolipoprotein B (apoB) that accepts cholesterol from macrophages using a fluorometric commercial kit (# K582-100, Bio Vision, CA, USA). To measure the cholesterol-accepting capacity of apoB-depleted serum, THP-1 monocytes (ATCC) were differentiated into macrophages by adding 100 nM of phorbol 12-myristate 13-acetate and incubating for 48 h. Approximately 1×10^5 cells per well were grown for 2 h in a 37 °C humidified 5% CO_2 incubator. The labeling reagent included in the kit was used to label cells and incubated overnight (16 h) in a 37 °C humidified 5% CO_2 incubator. After 16 h, the cells were gently washed with DMEM (without serum), and the medium was removed. ApoB-depleted serum [polyethylene glycol (PEG)-HDL prepared by mixing the serum with HDL cholesterol reagent (H751160, Pointe Scientific, USA) to obtain the supernatant] was applied to the cell as a cholesterol acceptor and incubated for 4 h. Fluorescence (excitation/emission = 482/515 nm) was measured for both the supernatant and cell lysate, and the % cholesterol efflux was calculated as the fluorescence intensity of the medium / (fluorescence intensity of the cell

lysate + fluorescence intensity of the media) × 100. To measure the cholesterol efflux capacity of ARPE-19 cells following treatment with AICAR, we replaced macrophages with ARPE-19 cells using the above procedure. The cholesterol efflux capacity of ARPE-19 cells was measured in the basal state, under the usual composition of culture media. Cells were labeled using the labeling reagent included in the kit and incubated overnight (16 h). Thereafter, cells were gently washed and treated with AICAR (0.5 mM) diluted in DMEM with 10% fetal bovine serum or media without AICAR and incubated for 16 h. After 16 h, fluorescence was measured, and the % cholesterol efflux was calculated in the same manner as described above.

8) Fundus examination and optical coherence tomography

The fundus of each mouse was examined for any subretinal deposits by applying a lubricant gel and a cover glass to the cornea under a surgical microscope. The optical coherence tomography angiography machine was available only at week 14 of the interim analysis. A swept source-based optical coherence tomography angiography prototype was used to assess the retinal vasculature and evaluate the outer retina and RPE. The detailed system specifications are provided in a previous study.[30]

We measured total retinal thickness (distance between the internal limiting membrane and RPE/BM complex) and outer retinal thickness (distance between the inner border of the outer nuclear layer and RPE/BM complex) from a horizontal optical coherence tomography scan approximately 200 μm above and below the optic disc using ImageJ.

9) Electron microscopy

The tissue was prepared as previously described.[31] The part including the optic nerve head and center of the retina was scanned at 40,000 × magnification. The thickness of the BM was measured in 10 spots from each selected image manually using ImageJ and then averaged. We also measured the proportion of EL particles in the BM using the threshold method in ImageJ. The EL particle index was calculated as the EL particle area/BM area ×100.

10) Statistical analyses

Data are presented as mean ± standard error of the mean. Data were normalized to that of the control group. The Mann-Whitney U and Kruskal-Wallis tests were used to compare the differences between the groups. PASW version 18.0 (SPSS, Inc., Chicago, IL) was used for statistical analysis. Statistical significance was set at $p < 0.05$.

RESULTS

1) **AICAR treatment increases the expression of the lipid transporters, ABCA1 and ABCG1, and cholesterol efflux in RPE cells in vitro**

We evaluated whether AICAR treatment influences lipid transporter expression in RPE cells and the cholesterol efflux capacity of cells. In the cell viability assay using ARPE-19 cells, more than 80% of cells were viable with treatment for up to 1 mM AICAR, whereas cell viability decreased below 60% of control with 2 mM AICAR treatment after 24 h (Fig. 1A). Cell viability decreased below 80% of the control after treatment with 10 μM Compound C (Fig. 1B). A combination of AICAR (0.5 mM) and Compound C (5 μM) resulted in over 80% cell viability after 24 h (Fig. 1C). Thus, we tested the cellular effect of AICAR (0.5 mM) and/or Compound C (5 μM).

Figure 1. Water-soluble tetrazolium salt-1 (WST-1) cell viability assay

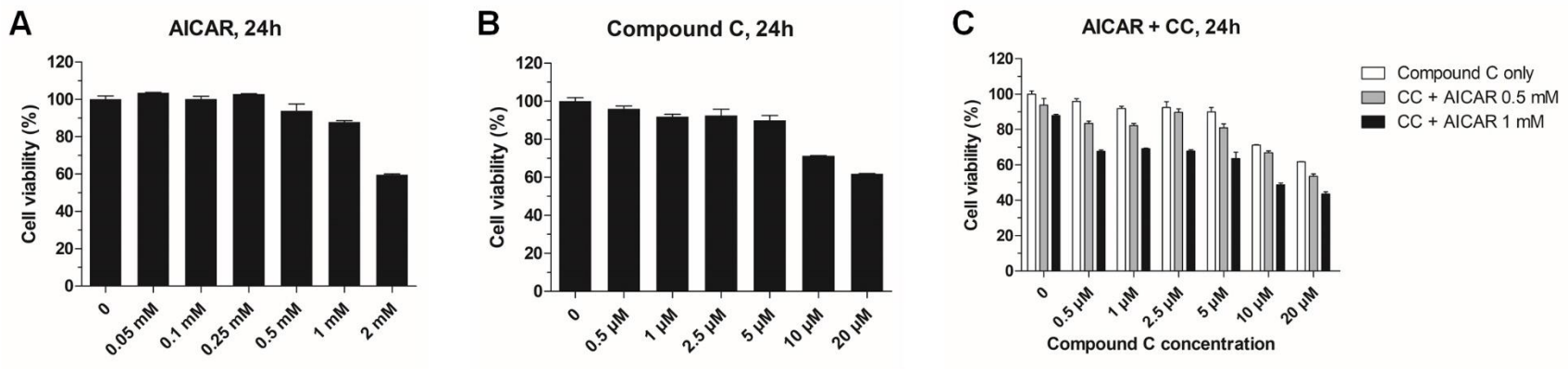

The viability of ARPE-19 cells after 24 h treatment with 5-aminoimidazole-4-carboxamide ribonucleotide (AICAR) and/or Compound C was evaluated using the WST-1 assay. (A) More than 80% of cells were viable on treatment with up to 1 mM AICAR, whereas cell viability decreased below 60% of control on treatment with 2 mM AICAR after 24 h. (B) Cell viability decreased below 80% of control on treatment with 10 μM Compound C. (C) Combined treatment with 0.5 mM of AICAR and 5 μM Compound C retained more than 80% of cell viability, and these concentrations were used further in this study to verify the cellular effect of AICAR and Compound C. Data are presented as the mean ± standard error of the mean for n = 3 per group.

AICAR treatment increased AMPK phosphorylation. The increased level of AMPK phosphorylation decreased with the addition of Compound C treatment; however, it was not significant. No significant differences in the amount of AMPK phosphorylation among the control, combined AICAR and Compound C treatment, and Compound C only treatment groups were noted. AICAR treatment increased the protein levels of ABCA1 and ABCG1. Increased expression of lipid transporters was diminished by the addition of Compound C treatment; however, it was not significant in ABCG1. No significant differences in the amount of SR-BI expression or the expression of an upstream transcription factor, LXR-α, were observed following treatment with AICAR and/or Compound C (Fig. 2A). ABCA1, ABCG1, and LXR-α mRNAs were upregulated in RPE cells after AICAR treatment, as revealed by qRT-PCR analysis (Fig. 2B). We measured the amount of fluorescence in the media, which was effluxed from RPE cells following AICAR or control treatment. AICAR treatment increased the cellular cholesterol efflux of ARPE-19 cells by 50% (Fig. 2C).

Figure 2. 5-aminoimidazole-4-carboxamide ribonucleotide (AICAR) treatment increases the expression of the lipid transporters, ABCA1 and ABCG1, and cholesterol efflux capacity in ARPE-19 cells

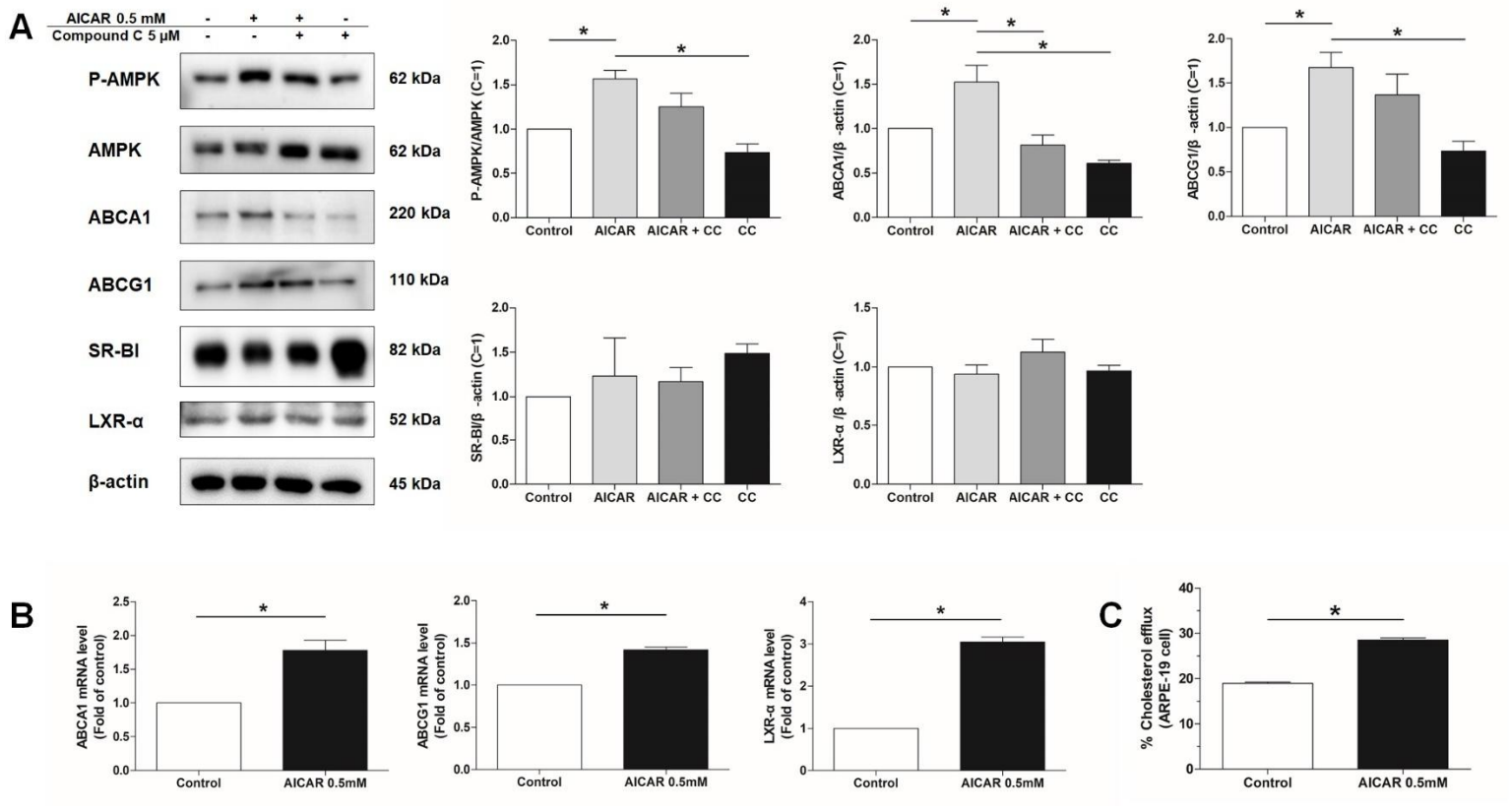

(A) AICAR treatment increases AMPK phosphorylation. The increased level of AMPK phosphorylation decreased with the addition of Compound C treatment; however, it was not significant. AICAR treatment increased the protein levels of ABCA1 and ABCG1. Increased levels of both ABCA1 and ABCG1 were diminished by treatment with Compound C; however, it was not significant in ABCG1. (B) Treatment with AICAR elevated the mRNA levels of ABCA1, ABCG1, and LXR-α. (C) AICAR treatment increased the cholesterol efflux capacity of ARPE-19 cells. Data are presented as the mean ± standard error of the mean for n = 4 per group from three independent experiments. Statistical analysis: *P < 0.05, Mann-Whitney U test.

A dose-dependent increase in the expression of lipid transporters, ABCA1 and ABCG1, and a corresponding increase in the cellular cholesterol efflux capacity of ARPE-19 cells after AICAR treatment were observed (Fig. 3).

Figure 3. A dose-dependent increase in lipid transporters and cholesterol efflux capacity in ARPE-19 cells following AICAR treatment

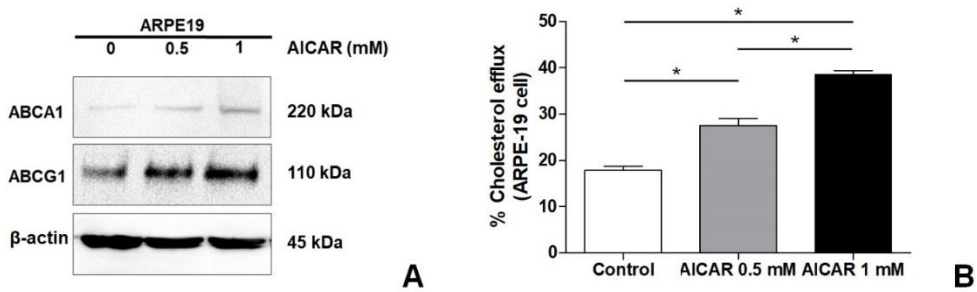

(A) There was a dose-dependent increase in the expression of lipid transporters ABCA1 and ABCG1 following AICAR treatment. (B) Cholesterol efflux capacity increased in a dose-dependent manner after AICAR treatment. Data are presented as mean ± standard error of the mean for n = 4 per group. *P < 0.05, Mann-Whitney U test.

2) **AICAR treatment increases the expression of the lipid transporters, ABCA1 and ABCG1, in the retina and RPE/choroid tissue in vivo**

We sought to determine whether AICAR treatment influences lipid transporter expression in the retina and RPE/choroid tissue of mice. The protein levels of the lipid transporters were elevated in the retinas of mice following AICAR treatment. The protein level of LXRα was also increased in AICAR-treated mice. However, no significant differences in SR-BI expression were noted among the three groups. The protein levels of phosphorylated acetyl-CoA carboxylase (ACC) in the retina of wild-type control mice and ApoE$^{-/-}$ mice were comparable. However, ApoE$^{-/-}$ mice treated with AICAR showed increased levels of phosphorylated ACC (Fig. 4A). The mRNA levels of ABCA1 (15-fold), ABCG1 (1.6-fold), and LXR-α (3.3-fold) in mice treated with AICAR. However, the basal level of ABCG1 mRNA in ApoE$^{-/-}$ mice was lower than that in control mice (0.3-fold). The basal level of ABCA1 mRNA in ApoE$^{-/-}$ mice was also lower than that in control mice (0.7-fold); however, this difference was not statistically significant (Fig. 4B).

Figure 4. 5-aminoimidazole-4-carboxamide ribonucleotide (AICAR) treatment increases the expression of the lipid transporters, ABCA1 and ABCG1, in the retina in vivo

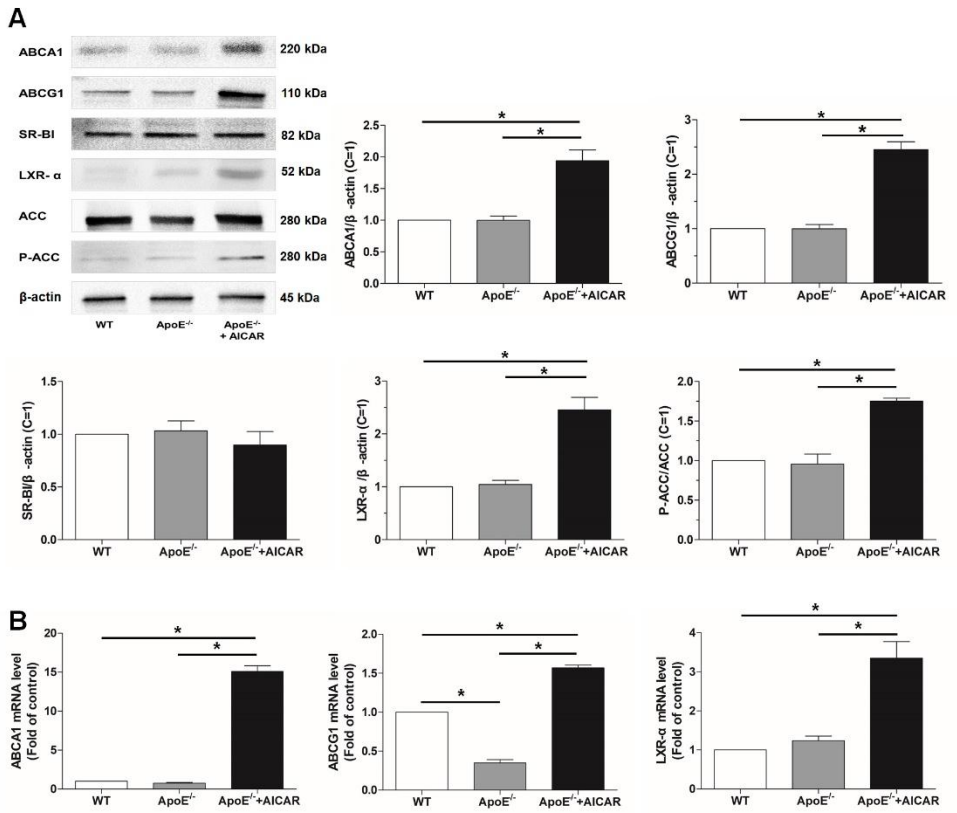

(A) AICAR treatment increased the protein expression of ABCA1, ABCG1, LXR-α, and phosphorylated ACC in the retina of $ApoE^{-/-}$ mice. (B) AICAR treatment upregulated the mRNA expression of ABCA1, ABCG1, and LXR-α in $ApoE^{-/-}$ mouse retinas. The basal mRNA level of ABCG1 in $ApoE^{-/-}$ mice that were not treated with AICAR were lower than those in control mice. Data are presented as the mean ± standard error of the mean for n = 4 per group from three independent experiments. Statistical analysis: *P < 0.05, Mann-Whitney U test.

The analysis using the RPE/choroidal tissue of mice showed comparable results to those from the retinal tissue. The ABCA1, ABCG1, LXR-α, and phosphorylated ACC protein levels were elevated in ApoE$^{-/-}$ mice treated with AICAR (Fig. 5A). The ABCA1 (3.2-fold), ABCG1 (3.5-fold), and LXR-α (4.9-fold) mRNA levels were higher in AICAR-treated mice than in control mice. However, basal mRNA expression levels of ABCA1 and ABCG1 in ApoE$^{-/-}$ mice that were not treated with AICAR were lower than those in control mice (0.7-fold and 0.15-fold, respectively, Fig. 5B).

Figure 5. 5-aminoimidazole-4-carboxamide ribonucleotide (AICAR) treatment increases the expression of the lipid transporters, ABCA1 and ABCG1, in the RPE/choroid tissue in vivo

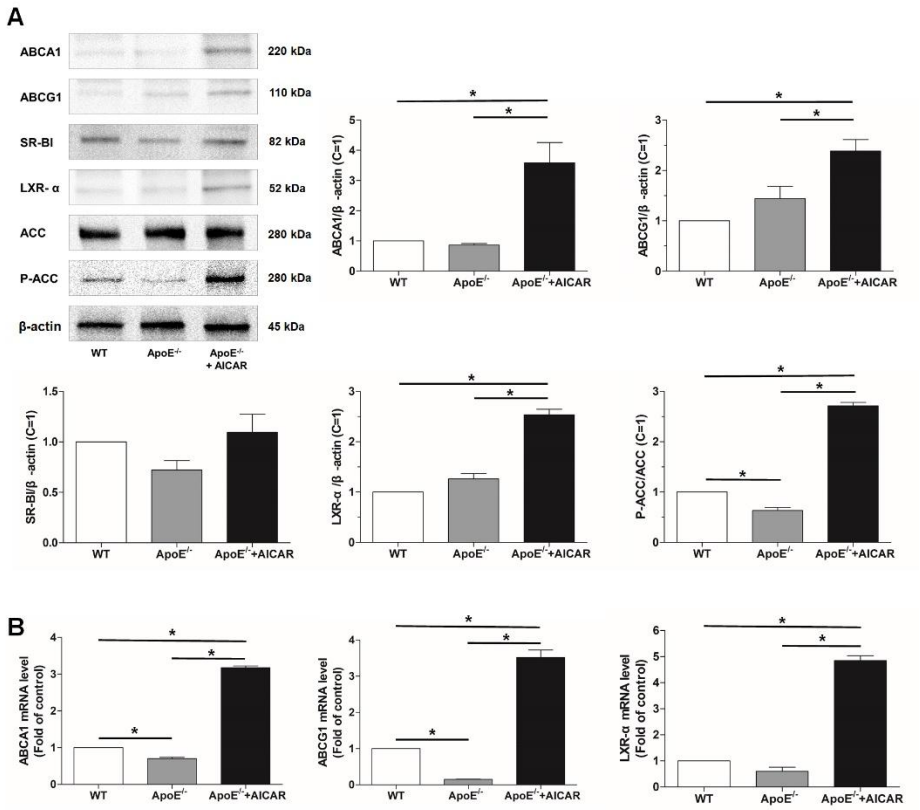

(A) AICAR treatment increased the protein expression of ABCA1, ABCG1, LXR-α, and phosphorylated ACC in the RPE/choroid tissue of $ApoE^{-/-}$ mice. (B) AICAR treatment increased the mRNA expression levels of ABCA1, ABCG1, and LXR-α in the RPE/choroid tissue of $ApoE^{-/-}$ mice. The basal mRNA levels of ABCA1 and ABCG1 in $ApoE^{-/-}$ mice that were not administered AICAR were lower than those in control mice. Data are presented as the mean ± standard error of the mean for n = 4 per group from three independent experiments. Statistical analysis: *$P < 0.05$, Mann-Whitney U test.

3) Serum lipid level and cholesterol accepting capacity of mice HDL

ApoE$^{-/-}$ mice had increased serum total cholesterol and LDL levels compared to that of the wild-type control mice. There were no significant differences in serum cholesterol levels between ApoE$^{-/-}$ mice treated and those not treated with AICAR (Fig. 6A). In this study, we sought to explore the role of reverse cholesterol transport in RPE pathophysiology; moreover, HDL cholesterol is known to be essential in this process. To evaluate HDL functionality, LDL and very LDL, which contain apoB, were precipitated from serum using PEG. We evaluated the cholesterol-accepting capacity of apoB-depleted serum (PEG-HDL) in mice by administering apoB-depleted serum to fluorescein-labeled lipid-laden macrophages and measuring the amount of effluxed fluorescein in the media. ApoB-depleted serum from ApoE$^{-/-}$ mice showed greater cholesterol-accepting capacity than that of wild-type control mice. Furthermore, the serum from mice treated with AICAR showed even greater cholesterol-accepting capacity than that of ApoE$^{-/-}$ mice that were not treated with AICAR (Fig. 6B).

Figure 6. Serum lipid level and high-density lipoprotein (HDL) cholesterol accepting capacity of mice

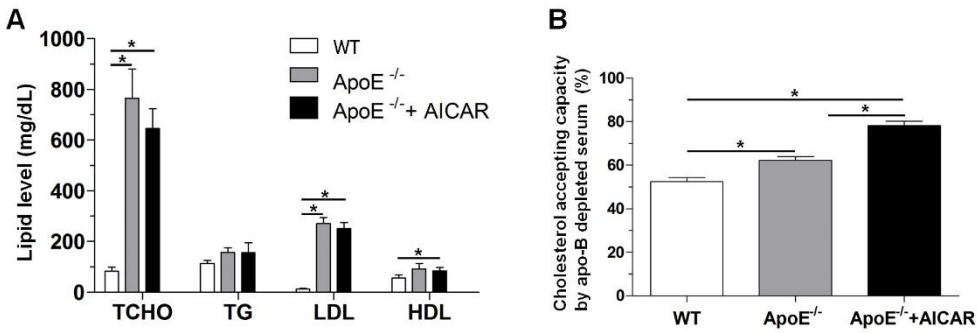

(A) ApoE$^{-/-}$ mice showed increased levels of serum total cholesterol and low-density lipoprotein (LDL) compared to control mice; however, no significant differences in serum cholesterol levels between ApoE$^{-/-}$ mice treated with 5-aminoimidazole-4-carboxamide ribonucleotide (AICAR) and those that were not treated with AICAR were noted. (B) ApoB-depleted serum of ApoE$^{-/-}$ mice showed greater cholesterol-accepting capacity than wild-type control mice. The serum of mice treated with AICAR showed even greater cholesterol-accepting capacity than that of ApoE$^{-/-}$ mice that were not treated with AICAR. Data are presented as mean ± standard error of the mean for n = 4 mice per group. Statistical analysis: *P < 0.05, and Mann-Whitney U test.

Abbreviations: TCHO, total cholesterol; TG, triglyceride; WT, wild type.

4) BM thickening and EL deposits were reduced after ApoE deficient mice were treated with AICAR

Fundus examination revealed no significant gross abnormalities, such as subretinal deposits, in any of the three groups at 24 weeks (Fig. 7). Furthermore, according to optical coherence tomography angiography, which was performed at 14 weeks, there were no significant vascular changes in the superficial and deep capillary plexus in $ApoE^{-/-}$ mice compared to control mice. Outer retinal and RPE examinations using optical coherence tomography revealed no significant abnormalities or retinal thickness changes in any group (Fig. 8 and Fig. 9).

Figure 7. Fundus findings in ApoE deficient mice and wild-type control mice

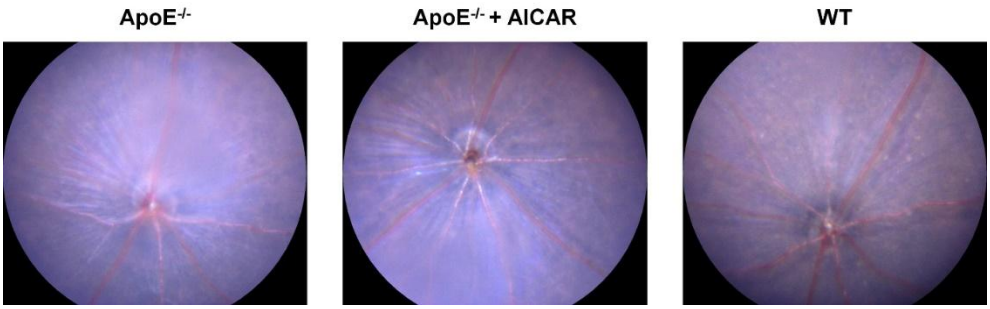

No significant gross abnormal findings, such as subretinal lipid deposits, were observed in the retinas of all three groups of mice.

Figure 8. Optical coherence tomography and optical coherence tomography angiography findings in mice at 14 weeks after treatment

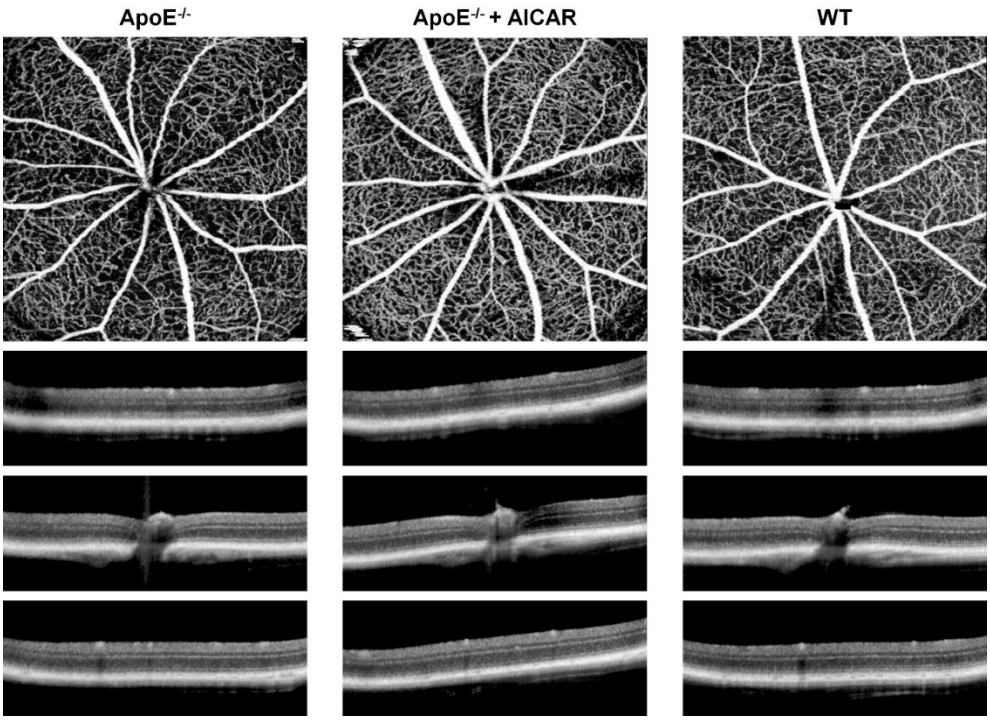

(Top row) Optical coherence tomography angiography of the superficial and deep capillary plexuses. (Bottom three rows) Horizontal optical coherence tomography scans at the level of the superior to the optic disc, optic disc level, and inferior to the optic disc approximately three-disc diameters apart from the optic disc, respectively. There were no significant vascular changes in the superficial and deep capillary plexuses in $ApoE^{-/-}$ mice compared to that of the control mice. Furthermore, no significant abnormalities were observed in the outer retinal or RPE levels in any of the three groups.

Figure 9. Comparison of retinal thickness among three groups

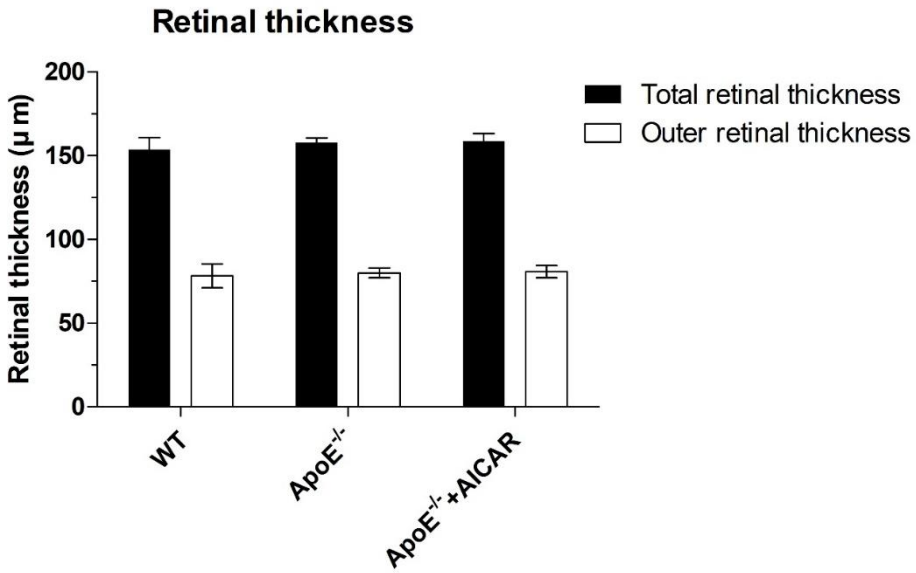

There were no significant differences in total retinal thickness (distance between the internal limiting membrane and RPE/BM complex) and outer retinal thickness (distance between the inner border of the outer nuclear layer and RPE/BM complex) among the three groups.

The structure of the BM was evaluated using electron microscopy. ApoE$^{-/-}$ mice had thicker BM than wild-type control mice at 14 and 24 weeks. ApoE$^{-/-}$ mice also showed greater accumulation of EL deposits in the BM. AICAR treatment significantly alleviated these pathological changes. Furthermore, no significant differences in terms of BM thickness and EL particle index were found between AICAR-treated ApoE$^{-/-}$ mice and control mice (Fig. 10).

Figure 10. Bruch's membrane (BM) thickening and electron-lucent deposits were reduced in ApoE deficient mice after 5-aminoimidazole-4-carboxamide ribonucleotide (AICAR) treatment

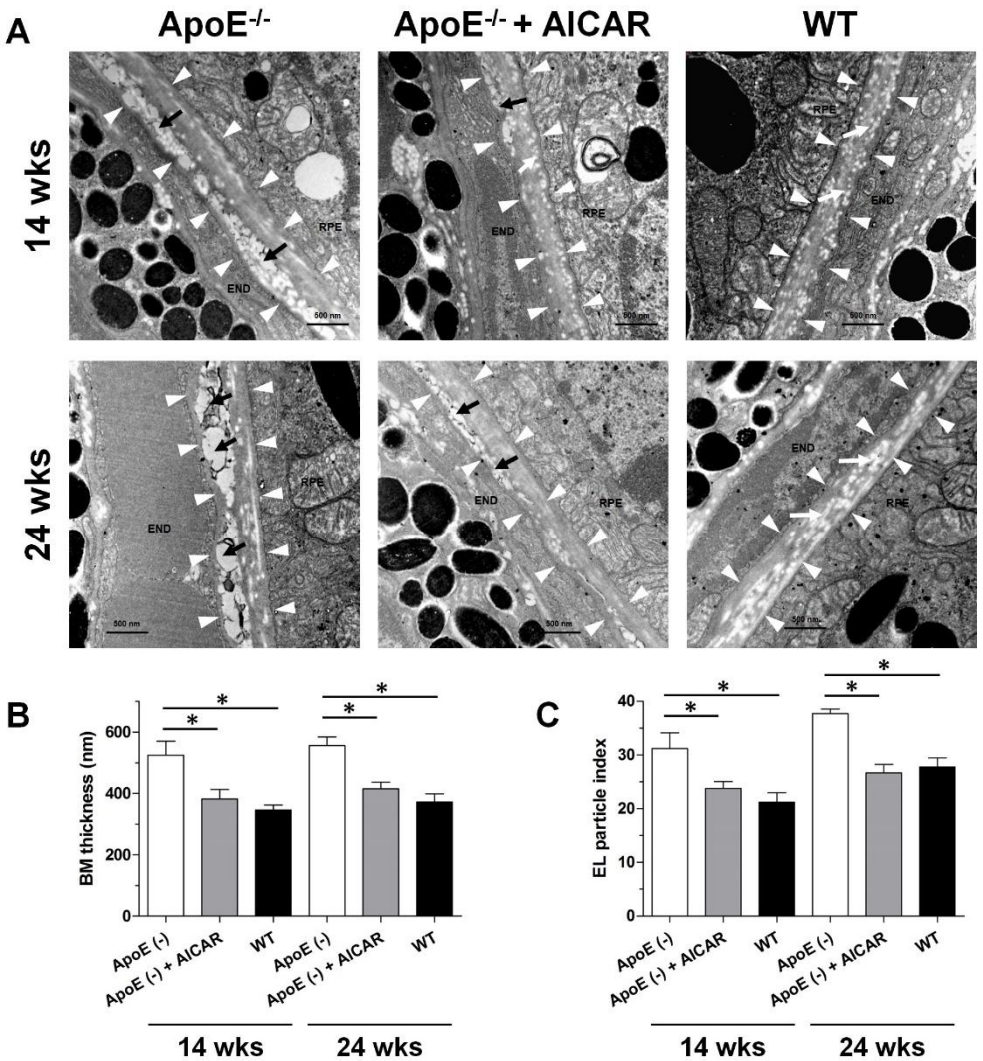

BM (between white arrowheads) is present between the retinal pigment epithelium and the endothelium of the choriocapillaris (END). ApoE$^{-/-}$ mice had a thicker BM than wild-type (WT) control mice at 14 and 24 weeks after treatment (A, white arrowheads). ApoE$^{-/-}$ mice also showed greater aggregation of electron-lucent (EL) deposits in the BM (A, black arrows). (B, C) AICAR treatment significantly

alleviated these pathologic changes, with no significant differences found in terms of BM thickness and EL particle index between AICAR-treated ApoE$^{-/-}$ mice and control mice. Data are presented as mean ± standard error of the mean for n = 3 mice per group. Three to four images from each mouse were obtained. Statistical analysis: *P < 0.05, and Mann-Whitney U test.

DISCUSSION

In this study, we investigated whether AICAR treatment could improve the cholesterol efflux capacity of RPE and reduce BM lipid deposits in ApoE$^{-/-}$ mice. AICAR treatment increased the expression of the lipid transporters ABCA1 and ABCG1 in the RPE in vitro and in vivo. It also upregulated ABCA1 and ABCG1 expression in retinal tissue. AICAR treatment improved the cholesterol efflux capacity of ARPE-19 cells and the ability of mouse serum HDL to accept cholesterol from macrophages. BM thickness and lipid deposition were reduced in ApoE$^{-/-}$ mice treated with AICAR.

Cholesterols are essential for various cellular processes; however, excess intracellular cholesterol is toxic to many cells. RPE plays a central role in lipid transport in the retina.[12] Circulating HDL and LDL enter the retina via class B scavenger receptors and LDL receptors in the RPE. RPE secretes apoB-containing lipoprotein particles basolaterally into the systemic circulation, presumably by diffusion and transcytosis.[12, 32] In this process, lipids may accumulate in the BM with aging, ultimately constructing a lipid layer, a precursor of basal linear deposits, and soft drusen.[12, 33]

ApoE$^{-/-}$ mice have high blood cholesterol levels, and thus might have high cholesterol influx into the RPE. As a result, the RPE will have to process more cholesterol. In these mice, as intracellular lipids are transported through the BM to the choriocapillaris, cholesterol accumulates in the BM, which increases the resistance to lipid transfer, ultimately resulting in BM thickening and lipid deposition. Interestingly, ApoE$^{-/-}$ mice treated with AICAR, which showed a higher expression level of lipid transporters, such as ABCA1, and theoretically would

have more extracellular cholesterol efflux, revealed less BM thickness and BM lipid deposition than those without AICAR treatment. The exact mechanism for reduced BM thickening and lipid deposition in ApoE$^{-/-}$ mice treated with AICAR is still elusive; however, we hypothesize that this could be explained as follows: First, the functionality of cholesterol acceptors, such as serum HDL, might have improved following AICAR treatment. HDL is known for its protective role against cardiovascular disease. Not only its quantity but its ability to accept cholesterol from macrophages are thought to be important in atheroprotection.[34, 35] According to previous studies, high HDL levels were associated with a greater risk of AMD.[36, 37] In this study, the cholesterol-accepting capacity of apoB-depleted serum from ApoE$^{-/-}$ mice was greater than that of control mice. This finding might be related to the greater HDL and associated content in ApoE$^{-/-}$ mice that could act as cholesterol acceptors. Interestingly, treatment with AICAR further increased the cholesterol-accepting capacity of HDL. In a previous study, pharmacological AMPK activation improved HDL functionality by improving the anti-inflammatory and antioxidative features of HDL in ApoE$^{-/-}$ mice. HDLs from mice treated with the AMPK activator showed greater cholesterol efflux from macrophages.[25] HDLs with more potent cholesterol-accepting capability will actively remove cholesterol effluxed from the RPE to the circulation, thereby preventing its deposition on the BM. In our pilot study, the ability of the serum to efflux cholesterol from macrophages was reduced in AMD patients compared to control patients, despite comparable serum lipid levels (unpublished data). On the other hand, a previous report suggested that the metrics of HDL composition and function were not associated with exudative AMD[38]; thus, further investigation is necessary to explore the role of HDL in the

pathogenesis of AMD.

Second, the beneficial effects of AICAR treatment that were not evaluated in this study may have affected the results. For example, the improvement in macrophage function by AMPK activation might alleviate BM pathology. In a previous study, AMPK activation enhanced ABCA1 expression in human macrophages via LXR-α activation and increased cholesterol efflux in macrophages.[22] Ban et al. reported that the targeted removal of macrophages ABCA1 and ABCG1 in mice led to BM thickening at six months.[19] AICAR is also known to induce autophagy, and macrophage-specific autophagy is important for cholesterol efflux from macrophage foam cells and reverse cholesterol transport.[39, 40]

AICAR is a widely used AMPK activator, and we believe that a significant portion of our findings is associated with AMPK activation by AICAR treatment. We found that AMPK phosphorylation was increased after AICAR treatment in ARPE-19 cells. Although not statistically significant, treatment with Compound C showed a trend toward reversing the effect of AICAR treatment. A higher concentration of Compound C may have a more definite AMPK inhibitory effect; however, it was difficult to perform such an experiment because of the cytotoxicity of the drug. ACC is phosphorylated by AMPK to inhibit enzyme activity when intracellular ATP is extensively utilized.[41, 42] We found that ACC phosphorylation was increased in the retinal and RPE tissues of mice treated with AICAR, which suggests that AMPK may be activated by AICAR treatment in these mice. However, AMPK-independent activity of AICAR, such as the mTOR signaling pathway, has also been reported.[43, 44] Further studies investigating the AMPK-independent pathways of AICAR related to lipid transport are needed.

There was a trend toward a decrease in mRNA levels of lipid transporters, ABCA1 and ABCG1, in retinal and RPE tissue of ApoE$^{-/-}$ mice compared to that of wild-type mice. However, there was no significant difference in protein levels. There is a possibility that western blotting may not have found a difference as sensitive as qRT-PCR, or there may be a post-transcriptional regulation such as reduced degradation of the protein to compensate for the deficiency in lipid transporters in ApoE$^{-/-}$ mice.

The association of upstream signaling pathways such as LXR-α after AICAR treatment in our study is inconclusive. We found increased mRNA levels of LXR-α in retinal and RPE/choroid tissue from mice and a corresponding increase in protein levels. However, in ARPE-19 cells, only an increase in mRNA levels was observed, without corresponding changes in protein levels. Previous studies on peritoneal macrophages from ApoE$^{-/-}$ mice revealed an increase in ABC transporters following pharmacological AMPK activation, without evidence of LXR-α activation, suggesting that a posttranscriptional mechanism may have been involved.[25] In contrast, treatment of peritoneal macrophages with an LXR agonist was found to induce a dose-dependent upregulation of ABC gene expression and restore the functional capacities of senescent macrophages, suggesting that the LXR pathway is important for ABC transporter regulation in macrophages.[45] A previous study using human macrophages showed an increase in ABCA1 expression through LXR-α activation following AMPK activation.[22] It seems that LXR-α may play a pivotal role in regulating ABC transporter expression; however, the LXR-α-independent mechanism at the post-transcriptional level is also expected to play a role in ABC transporter regulation.[46] Further research is needed

to determine the various mechanisms involved in the regulation of ABC transporter expression following AICAR treatment.

In this study, we only detected electron microscopic changes in the BM. In fact, we could not identify any gross retinal abnormalities, such as subretinal deposits, based on fundus examination. We used eight-week-old mice and examined them at 14 and 24 weeks after the initial treatment. There were no specific outer retinal-RPE or vascular abnormalities based on optical coherence tomography angiography examinations, possibly because of the limited axial resolution. ApoE$^{-/-}$ mice are known to display fundus lesions at 13 months of age; thus, we believe that the mice used in our study were relatively young for the occurrence of age-related retinal lesions. However, a previous electron microscopy study revealed relative thickening and lipid deposition in the BM of two-month-old ApoE$^{-/-}$ mice compared to control mice.[29] We believe that ultrastructural changes begin before apparent gross abnormalities in the RPE-BM complex, which may require early treatment to reverse the pathology.

Our study had several limitations. First, although we presented direct and indirect evidence of AMPK activation following AICAR treatment, the exact mechanisms involved in changes in lipid metabolism after AICAR treatment remain elusive. Furthermore, AMPK activation is known to be related to several beneficial effects other than improving cholesterol efflux function in retinal damage. AMPK activation is known to protect against retinal damage by increasing resistance to oxidative damage and mitochondrial biogenesis.[47] AMPK activation suppresses laser-induced choroidal neovascularization by inhibiting inflammatory cytokine levels and macrophage recruitment.[48] These effects would have had an overall

impact on our results. Second, our study lacked functional data, such as electroretinograms. Third, we were unable to measure the specific composition or the degree of Apo-B depletion in the serum used for cholesterol efflux measurement. Further studies on changes in the composition of HDL-associated apolipoproteins following AICAR treatment are needed. Fourth, we used a commercially available fluorometric method to evaluate the cholesterol efflux capacity instead of a radioactive isotope experiment. This fluorometric method is easier and safer than radioactive isotope experiment, as it does not require the handling of radioactive materials and enables the testing of a large number of samples. However, the results of the two methods must be compared to validate the methodology of cholesterol efflux capacity evaluation. Furthermore, we could not evaluate the cholesterol efflux capacity of RPE cells in vivo. A new technique to evaluate the RPE cholesterol efflux capacity in vivo is needed. Fifth, data on the effect of AICAR on control mice are lacking. The animals used in this study were relatively young and lacked age-related vascular or fundus changes. A previous study reported that BM lipid deposits are rarely observed even when a high-fat diet is administered to two-month-old mice.[49] Thus, it may be difficult to determine the treatment effect of AICAR on RPE and BM in young wild-type mice. Further studies on aged animals are needed to identify the effects of AICAR treatment on age-related lipid accumulation in the RPE and BM. Sixth, due to the limitation of an animal model used in our study, it was difficult to fully recapitulate the pathophysiology of dry AMD. It might be advantageous to use nonhuman primates models with a retinal structure similar to humans including the presence of a macula for more solid results,[50] which will also be useful for future clinical

applications.

CONCLUSIONS

AICAR treatment increased the expression of ABC lipid transporters in the retina and RPE of mice and facilitated intracellular cholesterol efflux from the RPE in vitro, possibly via AMPK activation. The ability of serum HDL to accept cholesterol effluxed from macrophages was also found to be improved following AICAR treatment. These effects seem to collectively contribute to improvements in age-related early BM pathologies, such as BM thickening and lipid deposition after treatment. Pharmacological improvement of RPE cholesterol efflux via AMPK activation may be a potential treatment strategy for AMD.

REFERENCES

1. Lim LS, Mitchell P, Seddon JM, et al. Age-related macular degeneration. Lancet 2012;379(9827):1728-38.

2. Chen W, Stambolian D, Edwards AO, et al. Genetic variants near TIMP3 and high-density lipoprotein-associated loci influence susceptibility to age-related macular degeneration. Proc Natl Acad Sci U S A 2010;107(16):7401-6.

3. Neale BM, Fagerness J, Reynolds R, et al. Genome-wide association study of advanced age-related macular degeneration identifies a role of the hepatic lipase gene (LIPC). Proc Natl Acad Sci U S A 2010;107(16):7395-400.

4. Reynolds R, Rosner B, Seddon JM. Serum lipid biomarkers and hepatic lipase gene associations with age-related macular degeneration. Ophthalmology 2010;117(10):1989-95.

5. Fauser S, Smailhodzic D, Caramoy A, et al. Evaluation of serum lipid concentrations and genetic variants at high-density lipoprotein metabolism loci and TIMP3 in age-related macular degeneration. Invest Ophthalmol Vis Sci 2011;52(8):5525-8.

6. McKay GJ, Patterson CC, Chakravarthy U, et al. Evidence of association of APOE with age-related macular degeneration: a pooled analysis of 15 studies. Hum Mutat 2011;32(12):1407-16.

7. Yu Y, Reynolds R, Fagerness J, et al. Association of variants in the LIPC and ABCA1 genes with intermediate and large drusen and advanced age-related macular degeneration. Invest Ophthalmol Vis Sci 2011;52(7):4663-70.

8. Fritsche LG, Chen W, Schu M, et al. Seven new loci associated with age-

related macular degeneration. Nat Genet 2013;45(4):433-9, 9e1-2.

9. Liu K, Chen LJ, Lai TY, et al. Genes in the high-density lipoprotein metabolic pathway in age-related macular degeneration and polypoidal choroidal vasculopathy. Ophthalmology 2014;121(4):911-6.

10. van Leeuwen EM, Emri E, Merle BMJ, et al. A new perspective on lipid research in age-related macular degeneration. Prog Retin Eye Res 2018;67:56-86.

11. Ruberti JW, Curcio CA, Millican CL, et al. Quick-freeze/deep-etch visualization of age-related lipid accumulation in Bruch's membrane. Invest Ophthalmol Vis Sci 2003;44(4):1753-9.

12. Curcio CA, Johnson M, Rudolf M, Huang JD. The oil spill in ageing Bruch membrane. Br J Ophthalmol 2011;95(12):1638-45.

13. Heinecke JW. The not-so-simple HDL story: A new era for quantifying HDL and cardiovascular risk? Nat Med 2012;18(9):1346-7.

14. Westerterp M, Bochem AE, Yvan-Charvet L, et al. ATP-binding cassette transporters, atherosclerosis, and inflammation. Circ Res 2014;114(1):157-70.

15. Duncan KG, Hosseini K, Bailey KR, et al. Expression of reverse cholesterol transport proteins ATP-binding cassette A1 (ABCA1) and scavenger receptor BI (SR-BI) in the retina and retinal pigment epithelium. Br J Ophthalmol 2009;93(8):1116-20.

16. Storti F, Grimm C. Active Cholesterol Efflux in the Retina and Retinal Pigment Epithelium. Adv Exp Med Biol 2019;1185:51-5.

17. Ban N, Lee TJ, Sene A, et al. Disrupted cholesterol metabolism promotes age-related photoreceptor neurodegeneration. J Lipid Res 2018;59(8):1414-23.

18. Storti F, Klee K, Todorova V, et al. Impaired ABCA1/ABCG1-mediated

lipid efflux in the mouse retinal pigment epithelium (RPE) leads to retinal degeneration. Elife 2019;8.

19. Ban N, Lee TJ, Sene A, et al. Impaired monocyte cholesterol clearance initiates age-related retinal degeneration and vision loss. JCI Insight 2018;3(17).

20. Hardie DG, Ross FA, Hawley SA. AMPK: a nutrient and energy sensor that maintains energy homeostasis. Nat Rev Mol Cell Biol 2012;13(4):251-62.

21. Chen B, Li J, Zhu H. AMP-activated protein kinase attenuates oxLDL uptake in macrophages through PP2A/NF-κB/LOX-1 pathway. Vascul Pharmacol 2016;85:1-10.

22. Kemmerer M, Wittig I, Richter F, et al. AMPK activates LXRalpha and ABCA1 expression in human macrophages. Int J Biochem Cell Biol 2016;78:1-9.

23. Guigas B, Sakamoto K, Taleux N, et al. Beyond AICA riboside: in search of new specific AMP-activated protein kinase activators. IUBMB Life 2009;61(1):18-26.

24. Ou HX, Huang Q, Liu CH, et al. Midkine Inhibits Cholesterol Efflux by Decreasing ATP-Binding Membrane Cassette Transport Protein A1 via Adenosine Monophosphate-Activated Protein Kinase/Mammalian Target of Rapamycin Signaling in Macrophages. Circ J 2020;84(2):217-25.

25. Ma A, Wang J, Yang L, et al. AMPK activation enhances the anti-atherogenic effects of high-density lipoproteins in apoE-/- mice. J Lipid Res 2017.

26. Klaver CC, Kliffen M, van Duijn CM, et al. Genetic association of apolipoprotein E with age-related macular degeneration. Am J Hum Genet 1998;63(1):200-6.

27. Souied EH, Benlian P, Amouyel P, et al. The epsilon4 allele of the

apolipoprotein E gene as a potential protective factor for exudative age-related macular degeneration. Am J Ophthalmol 1998;125(3):353-9.

28. Plump AS, Smith JD, Hayek T, et al. Severe hypercholesterolemia and atherosclerosis in apolipoprotein E-deficient mice created by homologous recombination in ES cells. Cell 1992;71(2):343-53.

29. Dithmar S, Curcio CA, Le NA, et al. Ultrastructural changes in Bruch's membrane of apolipoprotein E-deficient mice. Invest Ophthalmol Vis Sci 2000;41(8):2035-42.

30. Park JR, Choi W, Hong HK, et al. Imaging Laser-Induced Choroidal Neovascularization in the Rodent Retina Using Optical Coherence Tomography Angiography. Invest Ophthalmol Vis Sci 2016;57(9):Oct331-40.

31. Kim SH, Park S, Yu HS, et al. The antipsychotic agent clozapine induces autophagy via the AMPK-ULK1-Beclin1 signaling pathway in the rat frontal cortex. Prog Neuropsychopharmacol Biol Psychiatry 2018;81:96-104.

32. Tserentsoodol N, Gordiyenko NV, Pascual I, et al. Intraretinal lipid transport is dependent on high density lipoprotein-like particles and class B scavenger receptors. Mol Vis 2006;12:1319-33.

33. Curcio CA. Soft Drusen in Age-Related Macular Degeneration: Biology and Targeting Via the Oil Spill Strategies. Invest Ophthalmol Vis Sci 2018;59(4):Amd160-amd81.

34. Tall AR. Cholesterol efflux pathways and other potential mechanisms involved in the athero-protective effect of high density lipoproteins. J Intern Med 2008;263(3):256-73.

35. Khera AV, Cuchel M, de la Llera-Moya M, et al. Cholesterol efflux

capacity, high-density lipoprotein function, and atherosclerosis. N Engl J Med 2011;364(2):127-35.

36. Jonasson F, Fisher DE, Eiriksdottir G, et al. Five-year incidence, progression, and risk factors for age-related macular degeneration: the age, gene/environment susceptibility study. Ophthalmology 2014;121(9):1766-72.

37. Wang Y, Wang M, Zhang X, et al. The Association between the Lipids Levels in Blood and Risk of Age-Related Macular Degeneration. Nutrients 2016;8(10).

38. Pertl L, Kern S, Weger M, et al. High-Density Lipoprotein Function in Exudative Age-Related Macular Degeneration. PLoS One 2016;11(5):e0154397.

39. Hyttinen JM, Petrovski G, Salminen A, Kaarniranta K. 5'-Adenosine monophosphate-activated protein kinase--mammalian target of rapamycin axis as therapeutic target for age-related macular degeneration. Rejuvenation Res 2011;14(6):651-60.

40. Ouimet M, Franklin V, Mak E, et al. Autophagy regulates cholesterol efflux from macrophage foam cells via lysosomal acid lipase. Cell Metab 2011;13(6):655-67.

41. Angin Y, Beauloye C, Horman S, Bertrand L. Regulation of Carbohydrate Metabolism, Lipid Metabolism, and Protein Metabolism by AMPK. Exp Suppl 2016;107:23-43.

42. Lee M, Katerelos M, Gleich K, et al. Phosphorylation of Acetyl-CoA Carboxylase by AMPK Reduces Renal Fibrosis and Is Essential for the Anti-Fibrotic Effect of Metformin. J Am Soc Nephrol 2018;29(9):2326-36.

43. Rao E, Zhang Y, Li Q, et al. AMPK-dependent and independent effects of

AICAR and compound C on T-cell responses. Oncotarget 2016;7(23):33783-95.

44. Višnjić D, Lalić H, Dembitz V, et al. AICAr, a Widely Used AMPK Activator with Important AMPK-Independent Effects: A Systematic Review. Cells 2021;10(5).

45. Sene A, Khan AA, Cox D, et al. Impaired cholesterol efflux in senescent macrophages promotes age-related macular degeneration. Cell Metab 2013;17(4):549-61.

46. Su YR, Dove DE, Major AS, et al. Reduced ABCA1-mediated cholesterol efflux and accelerated atherosclerosis in apolipoprotein E-deficient mice lacking macrophage-derived ACAT1. Circulation 2005;111(18):2373-81.

47. Xu L, Kong L, Wang J, Ash JD. Stimulation of AMPK prevents degeneration of photoreceptors and the retinal pigment epithelium. Proc Natl Acad Sci U S A 2018;115(41):10475-80.

48. Nagai N, Kubota S, Tsubota K, Ozawa Y. Resveratrol prevents the development of choroidal neovascularization by modulating AMP-activated protein kinase in macrophages and other cell types. J Nutr Biochem 2014;25(11):1218-25.

49. Cousins SW, Espinosa-Heidmann DG, Alexandridou A, et al. The role of aging, high fat diet and blue light exposure in an experimental mouse model for basal laminar deposit formation. Exp Eye Res 2002;75(5):543-53.

50. Pennesi ME, Neuringer M, Courtney RJ. Animal models of age related macular degeneration. Mol Aspects Med. 2012;33(4):487-509.

초록

연령관련 황반변성의 원인은 다양하게 알려져 있는데, 최근에는 지질 대사의 이상이 그 주요 원인 중 한 가지로 제시되고 있다. ABCA1, ABCG1 등의 ABC 결합상자 수송체 (ATP-binding cassette transporters)는 고밀도지질단백을 생성하고, 대식세포의 콜레스테롤 유출을 조절하는데 중요한 역할을 하는 것으로 알려져 있다. 망막이나 망막색소상피세포의 콜레스테롤 유출 기능에 이상이 있을 경우 과도한 세포내 지질이 축적되며, 망막의 구조적, 기능적 손상을 일으킨다. 이번 연구에서는 일인산아데노신 활성화 단백질 인산화효소 (AMP-activated protein kinase, AMPK)를 활성화시키는 것으로 알려진 5-aminoimidazole-4-carboxamide ribonucleotide (AICAR) 약물이 망막색소상시세포의 콜레스테롤 유출능을 향상시키고, 부르크막의 지질 침착을 감소시킬 수 있는지 살펴보고자 한다. ARPE-19 세포주 및 ApoE 유전자 결손 마우스를 이용하여 AICAR 약물 처리 후 ABCA1, ABCG1 등의 지질 수송체의 단백질 및 mRNA 발현양에 변화가 있는지 살펴보았다. AICAR 약물 처리 후 ARPE-19 세포에서 콜레스테롤 유출능의 변화가 있는지, ApoE 유전자 결손 마우스의 혈청에서 콜레스테롤을 수용하는 능력에 변화가 있는지 분석하였다. ApoE 유전자 결손 마우스의 브루크막의 두께 및 지질 침착 정도를 전자 현미경을 이용하여 분석하였다. AICAR 약물 치료를 하였을 때 ARPE-19 세포에서 AMPK의 인산화가 증가하고, ABCA1, ABCG1 등의 단백질

및 mRNA 발현양이 증가하였으며, 콜레스테롤 유출능이 향상되었다. AICAR 약물 치료를 한 마우스의 망막 및 맥락막/망막색소상피 조직에서 ABCA1, ABCG1 등의 단백질 및 mRNA 발현양이 증가하였으며, 전자현미경 분석에서 브루크막의 두께 및 지질 침착이 감소하는 것을 확인할 수 있었다. 결론적으로, AICAR 치료는 ARPE-19 세포의 지질 수송체 발현을 증가시키고 콜레스테롤 유출능을 향상시켰으며, ApoE 유전자 결손 마우스의 망막 및 망막색소상피에서 지질 수송체의 발현을 증가시키고, 혈액의 콜레스테롤 수용 능력을 향상시켜, 궁극적으로 브루크막의 두께 및 지질 침착을 감소시켰다. AMPK를 활성화시키는 이러한 약물들은 추후 연령관련 황반변성의 새로운 치료 전략이 될 수 있을 것이다.

주요어: AICA 라이보뉴클리오타이드; 일인산아데노신 활성화 단백질 인산화효소; ABC 결합상자 수송체; 콜레스테롤; 황반 변성, 망막색소상피 세포

학번: 2014-30636

* 본 졸업 논문은 현재 Experimental Eye Research (Kim YK, Hong HK, Yoo HS, Park SP, Park KH, AICAR upregulates ABCA1/ABCG1 expression in the retinal pigment epithelium and reduces Bruch's membrane lipid deposit in ApoE deficient mice. Exp Eye Res. 2021 Dec;213:108854)에 출판 완료된 내용을 포함하고 있습니다.

* This research was supported by the Korean Association of Retinal Degeneration, the SK Telecom Research Fund [grant number 06-2014-160], and the Basic Science Research Program through the National Research Foundation of Korea (NRF) funded by the Ministry of Science and ICT [grant numbers 2018R1A2B6007809, 2021R1F1A1057121]. The funding organization had no role in the design or conduct of this study.